Int. J. Environ. Sci. Technol. (2016) 13:849–856
DOI 10.1007/s13762-015-0909-8

ORIGINAL PAPER

# Study of photocatalytic degradation of environmentally harmful phthalate esters using Ni-doped $TiO_2$ nanoparticles

**P. Singla[1] · O. P. Pandey[1] · K. Singh[1]**

Received: 1 June 2015 / Revised: 28 September 2015 / Accepted: 11 November 2015 / Published online: 24 November 2015


**Abstract** Undoped and Ni-doped $TiO_2$ nanoparticles are synthesized using sol–gel technique. The physical, structural, optical and thermal properties of the samples are investigated using X-ray powder diffraction, Fourier transform infrared spectroscopy, transmittance electron microscopy, UV–visible diffuse reflectance and thermogravimetric analysis. The photocatalytic activity of the samples is investigated by the photocatalytic degradation of phthalate esters. Phthalate esters have been considered as endocrine disrupting compounds. Ni-doped $TiO_2$ samples show better photocatalytic activity as compared to undoped $TiO_2$ sample. The greater photocatalytic activity of doped samples as compared to undoped $TiO_2$ can be attributed to the production of more number of electron–hole pairs in doped samples.

**Keywords** Sol–gel process · X-ray methods · Optical properties · $TiO_2$ · Photocatalytic activity

## Introduction

Water contamination has become a serious problem on the global scale, and millions of the people lack access to clean water sources. A large number of products made of organic chemicals are used daily in order to improve the quality of life. Wastewater effluents containing organic chemicals, released by various industries, factories, laboratories, etc., contaminate the water bodies to a greater extent. The important organic pollutants include dyes, pesticides, insecticides, pharmaceutical medicines, herbicides, hydrocarbons, phenols, phthalate esters, etc. (Wang et al. 2014). Phthalate esters are used as plasticizers to increase the flexibility of the materials. They are used in flooring, paints, lubricants, wallpapers, toys, cosmetics, medical products, plastic packing films, electronic, auto products, etc. (Fairbairn et al. 2012).

Phthalate esters have been detected in appreciable quantities in river water, waste water, drinking water and sediments in environment across the world (Nahum et al. 2013). The United States Environmental Protection Agency (US EPA) and some of its counterparts have classified the most common phthalate esters as priority pollutants and hormone disrupting compounds (Cheng 2012). Phthalate esters may seriously harm human respiratory, reproductive and endocrine systems. Incorporating phthalate esters into a polymer matrix reduces the glass transition temperature of the polymer. Phthalate esters are not bound to the polymer with covalent bonds and are therefore able to migrate to the surface of the polymer matrix where they may be lost by a variety of physical processes (Staples 2003).

Heterogeneous photocatalytic degradation using $TiO_2$-based photocatalysts is frequently used for the complete degradation of organic pollutants using visible and UV radiation as energy sources (Singla et al. 2014). This works on the principle that when light falls on the surface of $TiO_2$, there is a generation of electron–hole pairs. The photogenerated electron–hole pairs react with water adsorbed on the surface of sample and oxygen. This reaction produces hydroxyl radicals and superoxide ions, respectively (Abbad et al. 2012). The hydroxyl radicals and superoxide ions are highly reactive to degrade organic pollutants (Singla et al. 2014). Recently, Kaur et al. (2015) used visible light active $TiO_2$ for photocatalytic degradation of different reactive dyes like Reactive Red 198, Reactive Blue 4, Reactive Black 5 and Reactive Orange 16. Ananpattarachai and

✉ K. Singh
kusingh@thapar.edu

[1] School of Physics and Materials Science, Thapar University, Patiala, Punjab 147004, India

Kajitvichyanukul (2015) degraded p,p′-DDT under UV and visible light using Ni-doped $TiO_2$. Jamil et al. (2015) used nanosized $TiO_2$ for degradation of phenol enriched water by solar photocatalytic oxidation. There are many reports available in the literature related to degradation of organic pollutants using $TiO_2$. From the thorough study of literature, it can be said that maximum work has been carried out on degradation of colored compounds like dyes. Photocatalytic degradation of colorless compounds like phthalate esters needs to be exposed more since dyes are not the only pollutants present in water. Photocatalytic degradation technique is gaining importance due to its many advantages over the competing processes such as complete mineralization, low cost, mild temperature and pressure conditions and no secondary pollution problems (Chong et al. 2010).

$TiO_2$ has been considered as a suitable photocatalyst for wastewater treatment. $TiO_2$ is a widely used material owing to its stability, nontoxicity, inexpensiveness, biocompatibility, biological and chemical inertness, strong oxidizing power and photocatalytic efficiency (Suwanchawalit et al. 2012; Liu et al. 2009). However, due to its large band gap, it can be excited under UV irradiation only. Second, in $TiO_2$ there is a high rate of electron–hole recombination, which decreases its photocatalytic activity (Wang et al. 2012). Doping $TiO_2$ with transition metals is an efficient method to extend the absorption of $TiO_2$ into the visible region and increasing its photocatalytic activity (Tain et al. 2012). Hence, researchers have doped many transition metals like Cr, Mn, Co, Mo, Ni, Cu and Zn into $TiO_2$ to modify its band gap and photocatalytic activity (Zaleska 2008; Ghasemi et al. 2009). There are many methods available to synthesize undoped and doped $TiO_2$ photocatalysts. Sol–gel technique is one of the most used methods to synthesize $TiO_2$-based photocatalysts due to its low cost, low temperature requirement, simplicity and high potential for controlling the bulk and surface properties of the oxides (Uddin et al. 2012; Akpan and Hameed 2010).

Research has been carried out related to the degradation of phthalate esters by many methods (Xu et al. 2013; Sarkar et al. 2013; Wu et al. 2013; He et al. 2013). Very few reports are available in the literature related to the degradation of phthalate esters using $TiO_2$-based photocatalytic degradation (Jiana et al. 2013; Jing et al. 2011; Ding et al. 2008). To the best of our knowledge, there is no report related to the degradation of phthalate esters using Ni-doped $TiO_2$ nanoparticles. Many researchers have doped Ni into $TiO_2$ by various processing methods to increase photocatalytic activity of $TiO_2$ (Nakhate et al. 2010; Woo et al. 2007; Ganesh et al. 2012). The present work focuses on the synthesis of undoped and Ni-doped $TiO_2$ nanoparticles by the sol–gel method. The synthesized powders are further used to degrade diethyl phthalate and dimethyl phthalate esters through photocatalytic degradation technique. Both these phthalate esters are highly conjugated systems which increase their persistence in the environment. The degradation study of phthalate esters is performed in the laboratory.

## Materials and methods

### Materials

All the chemicals are used in pristine form without any further purification, and doubly distilled water is used in all the experiments. The chemicals procured and used are titanium isopropoxide (Sigma-Aldrich, 97 %), anhydrous ethanol (Merck, 99.9 %), nickel nitrate hexahydrate (Himedia, 97.0 %), nitric acid (Merck, 69–72 %) and diethyl phthalate (sd fine chem., 99.0 %).

### Preparation of photocatalysts

Undoped and nickel-doped $TiO_2$ nanoparticles are prepared by the sol–gel technique. The precursors used are titanium(IV) isopropoxide and nickel nitrate hexahydrate. Titanium isopropoxide is mixed with anhydrous ethanol in a molar ratio of 1:25, and the solution is stirred for 30 min. The above-prepared solution is added dropwise to the second solution containing distilled water, anhydrous ethanol, nitric acid and nickel nitrate hexahydrate. The molar ratio of nitric acid, anhydrous ethanol and distilled water in second solution is 1:3.6:4.2. The molar ratio of $Ni^{2+}/Ti^{4+}$ in different samples varies from 0.2 to 0.6 mol%. After complete addition, a transparent color sol is obtained. Furthermore, the sol is magnetically stirred for 2 h to obtain the gel. The gel is kept for aging for 1 day, and then aged gel is dried at 100 °C. The dried solid is ground in an agate mortar to obtain a fine as well as homogeneous powder. Finally, the obtained powder is calcined at 450 °C for 2 h. Undoped $TiO_2$ nanoparticles are prepared using the similar method as prescribed above except in the absence of nickel nitrate hexahydrate. The synthesis of samples by above described method followed the work of Chen et al. 2008. Undoped, 0.2, 0.4 and 0.6 mol% Ni-doped $TiO_2$ samples are labeled as T0N, T2N, T4N and T6N, respectively.

### Characterization of photocatalysts

X-ray powder diffraction analysis is carried out using PANalytical's X'Pert Pro X-ray diffractometer with Cu Kα radiations ($\lambda = 1.54$ Å) with working voltage and current of 45 kV and 40 mA, respectively. The patterns were recorded over the angular range of 20°–80°. During experimentation, the step size was 0.0130°. The infrared spectra of the samples are recorded on FTIR Spectrometer Model RZX (PerkinElmer) using KBr pellets. The resolution of the FTIR instrument was 1 $cm^{-1}$ and scan range of 4000–250 $cm^{-1}$. To study the absorption spectra of the photocatalysts, the

diffuse reflectance spectra (DRS) of the samples are obtained using UV–Vis spectrophotometer (Hitachi U-3900H) in spectral range of 250–800 nm. The scan speed and sampling interval during scan are 300 nm/min and 0.50 nm, respectively. The morphology and size of nanoparticles are characterized using transmission electron microscope (Hitachi, H-7500) operated at an accelerating voltage of 80 kV. The prepared samples are dissolved in ethanol, and drop of colloids is put on the copper grid for TEM measurement. Thermal analysis is carried out with the help of NETZSCH Jupiter STA 449 F3 simultaneous thermal analyzer in argon atmosphere with heating rate of 10 °C/min from 25 to 800 °C. The photocatalytic activity of the samples is measured in terms of the degradation of diethyl phthalate. The extent of diethyl phthalate degradation is monitored using UV–Vis spectrophotometer (Hitachi U-3900H).

### Photocatalytic reaction experiment

The photocatalytic degradation of diethyl phthalate is carried out in a three-jacketed column photoreactor (shown in Fig. 1) made up of borosilicate glass with an effective volume of 100 ml. The three jackets of photoreactor are used individually for circulating water to maintain the temperature, for the lamp and for the reaction mixture. A mercury lamp of 125 W ($\lambda = 365$ nm) having intensity 40,000 lux is placed axially inside the photoreactor. The experimental conditions are fixed at 30 ppm diethyl phthalate solution and catalyst loading of 1 g/l. Prior to photoreaction, the suspension is magnetically stirred in dark condition for 30 min to establish absorption/desorption equilibrium condition. Likewise during the photocatalytic reaction, the aqueous suspension is magnetically stirred. Aliquots of mixture are taken out at periodic intervals during the irradiation and then filtered through Millipore syringe filters (PTFE, 0.45 μm). The photocatalytic degradation of diethyl phthalate is determined by a UV–Vis spectrometer on the basis of Beer–Lambert law.

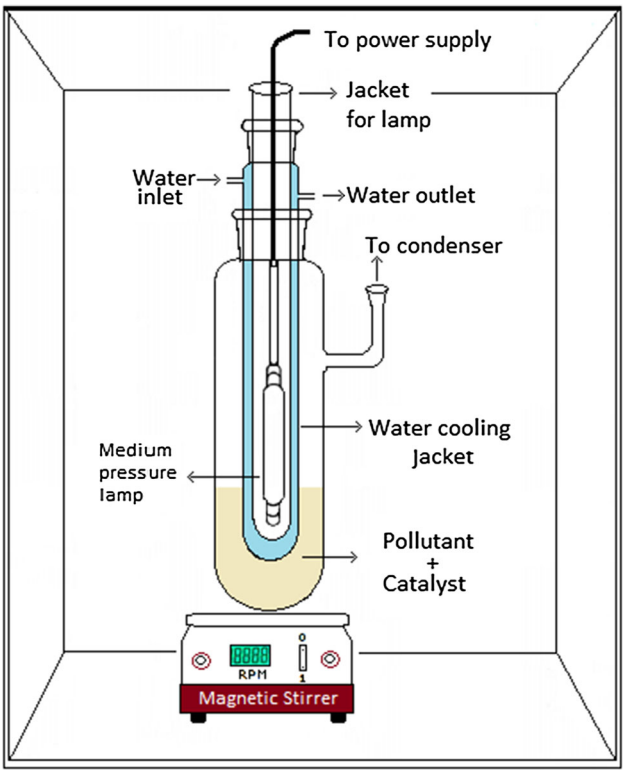


**Fig. 1** Schematic representation of experimental setup

## Results and discussion

### XRD analysis

X-ray diffraction patterns of undoped and Ni-doped $TiO_2$ nanoparticles calcined at 450 °C are shown in Fig. 2. The XRD patterns of the samples show the presence of two phases, namely anatase (ICDD No. 01-089-4921) and rutile (ICDD No. 01-083-2242). The diffraction peaks at $2\theta = 25.36°$, 36.9°, 37.8°, 38.5°, 48.0°, 53.8°, 55.0°, 62.7°, 70.3° and 75.1° are attributed to the anatase phase of $TiO_2$. The diffraction peaks at $2\theta = 27.4°$, 36.0°, 39.1°, 41.2°, 44.0°, 54.3°, 56.6°, 64.0° and 69.2° are attributed to rutile phase of $TiO_2$. The XRD peaks at $2\theta = 25.36°$ (101) and $2\theta = 27.4°$ (110) are

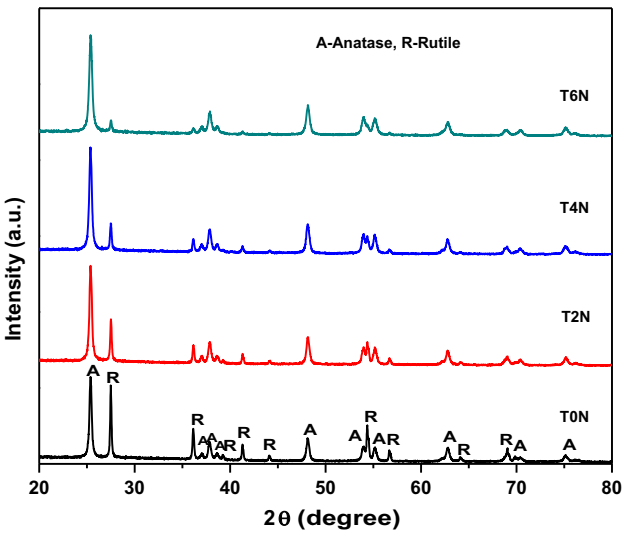


**Fig. 2** XRD patterns of undoped and Ni-doped $TiO_2$ nanoparticles calcined at 450 °C

taken as characteristic peaks for anatase and rutile phases, respectively. The volume fraction of anatase phase increases with doping as given in Table 1. From Fig. 2, it is clear that intensity of all the peaks corresponding to the rutile in doped $TiO_2$ samples decreases with increasing amount of dopant, which indicates the inhibition of rutile phase due to doping of nickel. Same dopant in substitutional form may increase the

**Table 1** XRD study of undoped and Ni-doped $TiO_2$ nanoparticles calcined at 450 °C

| Sample Id | Crystallite size (nm) | Volume percentage | | Lattice constants | Cell volume (Å)$^3$ |
|---|---|---|---|---|---|
| | | Anatase | Rutile | | |
| T0N | 28 | 67.2 | 32.8 | $a = b = 3.78$ Å, $c = 9.28$ Å | 132.59 |
| T2N | 27 | 79.5 | 20.5 | $a = b = 3.78$ Å, $c = 9.49$ Å | 135.59 |
| T4N | 25 | 86.4 | 13.6 | $a = b = 3.78$ Å, $c = 9.49$ Å | 135.59 |
| T6N | 22 | 95.2 | 4.8 | $a = b = 3.78$ Å, $c = 9.28$ Å | 132.59 |

oxygen vacancy level and thereafter promote the phase transformation, whereas in the interstitial form, it may enhance lattice constraint and hence inhibit the phase transformation. This concept usually applies to all the dopants, although the transition metal ions like Mn, Fe and Ni with variable valency mostly show mixed effects (Hanaor and Sorrell 2011). As phase transformation is getting inhibited in the present case, Ni is expected to occupy interstitial site in the synthesized samples. Generally, the presence of interstitial ions as well as the reduction in interparticle contact (grain boundary phases) in anatase phase inhibits the transformation (Hanaor and Sorrell 2011). The crystallite size is estimated using Debye–Scherrer formula (Devi et al. 2010):

$$D = \frac{K\lambda}{\beta \cos\theta} \quad (1)$$

where $D$ is the crystallite size, $K$ the shape factor, $\lambda$ the wavelength, and $\beta$ full width at the half maximum. The crystallite size of T0N, T2N, T4N and T6N samples is obtained to be approximately 28, 27, 25 and 22 nm, respectively. Moreover, the crystallite size decreases with the increase in dopant concentration, which can be attributed to the peak broadening due to defects created by dopant in doped samples. In addition to this, no characteristic peak corresponding to Ni has been observed, which may be due to the fine dispersion of metal particles on $TiO_2$ or very small metal content (Vijayan et al. 2009).

## DRS analysis

Diffuse reflectance spectroscopy (DRS) has been used to study the optical properties of the samples. Using DRS, it is possible to study the optical properties of the samples in powdered state. Effects of light scattering in the absorption spectra of powdered samples dispersed in liquid can be avoided using DRS. DRS works on the focused projection of spectrometer beam into the sample, where it is reflected, scattered and transmitted through the sample. The back-reflected, diffusely scattered light (some of which is absorbed by the sample) is then collected by the accessory and directed to detector optics (Ebraheem and Antar 2013). Figure 3 shows the diffuse reflectance spectra of undoped and Ni-doped $TiO_2$

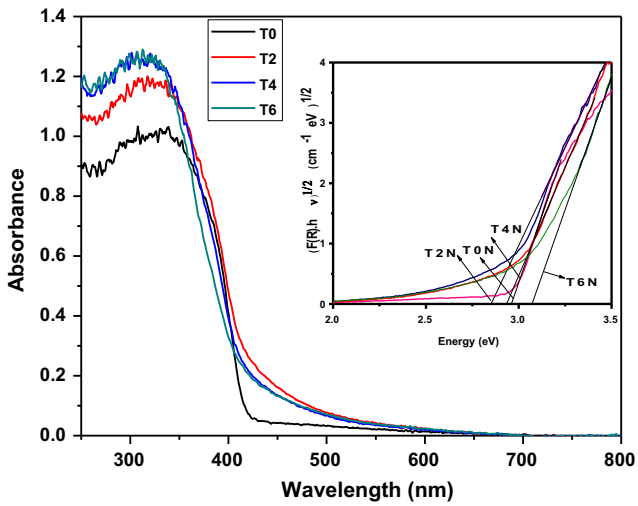


**Fig. 3** UV–Vis absorption spectra of undoped and Ni-doped $TiO_2$ nanoparticles calcined at 450 °C

samples measured in the UV–Vis region. It clearly indicates that the doped samples show remarkable absorbance in the region of 400–550 nm, demonstrating their strong visible light absorbance ability as compared to the undoped sample. The band gap of the samples is calculated using Kubelka–Munk function which is $f(R) = (1 - R)^2/2R$, where $R$ is the diffuse reflectance (Umar et al. 2013). In the present case, $(f(R)\cdot h\nu)^{1/2}$ is plotted against photon energy $h\nu$ (shown in inset of Fig. 3) and the linear portion of the curves is extrapolated to have an intercept on the x-axis. The value at $x$-axis where intercept cuts, i.e., $(f(R)\cdot h\nu)^{1/2} = 0$, is taken as the value of the band gap. For the linear region of the plots, the following relationship must be satisfied:

$$[f(R) \cdot h\nu]^{1/2} = K\left(h\nu - E_g\right) \quad (2)$$

where $E_g$ is band gap energy and $K$ is a characteristic constant for every semiconductor material (Umar et al. 2013). The band gap of T0N, T2N, T4N and T6N samples is obtained to be 2.94, 2.87, 2.97 and 3.07 eV, respectively. Pure anatase has band gap of 3.2 eV, whereas for rutile phase, it is 3.0 eV. However, a mixture of these phases yields lower band gap corresponding to the visible region (Aguilar et al. 2013). In general, anatase is considered to be a better photocatalyst than

the rutile, but the mixture of both yields the best photocatalytic activities. Mixture of both the phases of titania is advantageous for photocatalytic activity due to synergistic effect of different phases. The results obtained for the present studies are in correlation with this explanation already in the literature given (Aguilar et al. 2013).

The redshift of 0.2 mol% Ni–$TiO_2$ samples can be attributed to the charge transfer transitions between impurity band and the $TiO_2$ conduction band (Paul and Choudhary 2014). In $TiO_2$, the valence band is composed of O-2*p* states and the conduction band is composed of Ti-3*d* states. The incorporation of $Ni^{2+}$ into $TiO_2$ lattice host provides Schottky barriers, which facilitate the transfer and trapping of electrons from $TiO_2$. Hence, the charge transfer between the $Ni^{2+}$ ions d-electron and $TiO_2$ conduction will appear (Paul and Choudhary 2014). The $Ni^{2+}$ ions could make significant changes on the structure of a crystalline material and thus on the values of gap energy. The effect due to modification of the band structure of $TiO_2$ by Ni can be verified by determining the material Urbach energy before and after introduction of the dopant. Urbach energy gives a measure of structural disorder in a material and is given by the tail region where absorption $\alpha$ ($v$) depends exponentially on the photon energy hν as follows (Hajjaji et al. 2014):

$$\alpha = \alpha_0 \exp\left\{\frac{(h\nu)}{E_u}\right\} \quad (3)$$

where $E_u$ is the Urbach energy. Absorption coefficient is proportional to $f(R)$; hence, $E_u$ is calculated by plotting ln $f(R)$ versus $h\nu$. The reciprocal of the slopes of the linear portion gives the value of $E_u$. The Urbach energy of T0N, T2N, T4N and T6N samples is 0.038, 0.098, 0.098, 0.150 eV, respectively. Higher Urbach energy in doped samples depicts more disorder in them as compared to the undoped samples (Kaur et al. 2012). Many factors like dislocations, electric field of defects and thermal vibrations can cause the tailing of energy states in the forbidden gap. According to Dow and Redfield, Urbach energy is attributed to the random internal electric field associated with the structural disorder, which broadens the excitons line (Mansour et al. 2007). Tauc and Menth (1972) explained disordering to be the transitions between the localized states in the band edge tails where the density is assumed to fall exponentially.

## FTIR analysis

The FTIR patterns for all the samples are shown in Fig. 4. To improve the visibility of the bands, FTIR patterns of the samples are plotted in finger print region of 1300–400 $cm^{-1}$. In all the samples, the group frequency region of 4000–1300 $cm^{-1}$ (not shown in figure) has bands around 3300–3450 and 1620–1635 $cm^{-1}$ which are attributed to the stretching vibrations of O–H groups and bending vibrations of adsorbed water

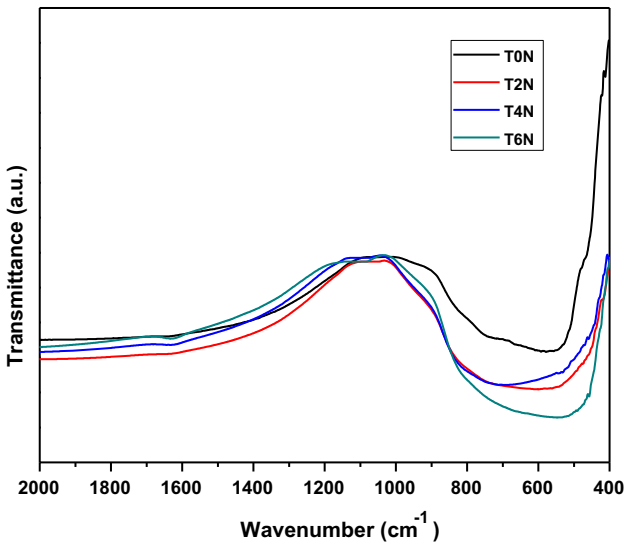


**Fig. 4** FTIR patterns of undoped and Ni-doped $TiO_2$ nanoparticles calcined at 450 °C

molecules, respectively (Loan and Long 2014). Moreover, occurrence of bands between 1300–1500 and 2800–3000 $cm^{-1}$ indicates the presence of small amount of organic material in the sample (Kumaresan et al. 2011; Yang et al. 2006). The absorption bands in a recorded IR spectrum have three important parameters, i.e., frequency, shape and intensity. Any deviation in band frequency, shape or intensity between the two spectra indicates the difference between the two samples. All single absorption bands by nature are symmetric in shape and have shape that resembles a normal bell curve. Deviation in band shape is related to similar function group that exists in different molecular environment. The presence of asymmetric band also indicates that sample is a mixture or has been modified. The width of band can be increased by inter- or intramolecular bond. In present case, band around 500 $cm^{-1}$ is due to stretching vibrations of Ti–O–Ti and Ti–O bonds (Venkatachalam et al. 2007). It is obtained that the band around 500 $cm^{-1}$ has different shape in case of doped sample as compared to undoped sample due to modification. Moreover, the band is shifting toward lower wavenumber in case of doped samples. This indicates the weakening of bonds. With the introduction of dopant, the structural rearrangements can take place in Ti–O–Ti environment leading to strained network and distortion of local symmetry. The band is more intense in case of doped samples as compared to undoped because of the presence of more molecules in doped samples. Our results agree well with the results obtained by Ganesh et al. (2012) also.

## TEM analysis

TEM micrographs of undoped and 0.6 mol% Ni-doped $TiO_2$ samples are shown in Fig. 5. The particle size of undoped

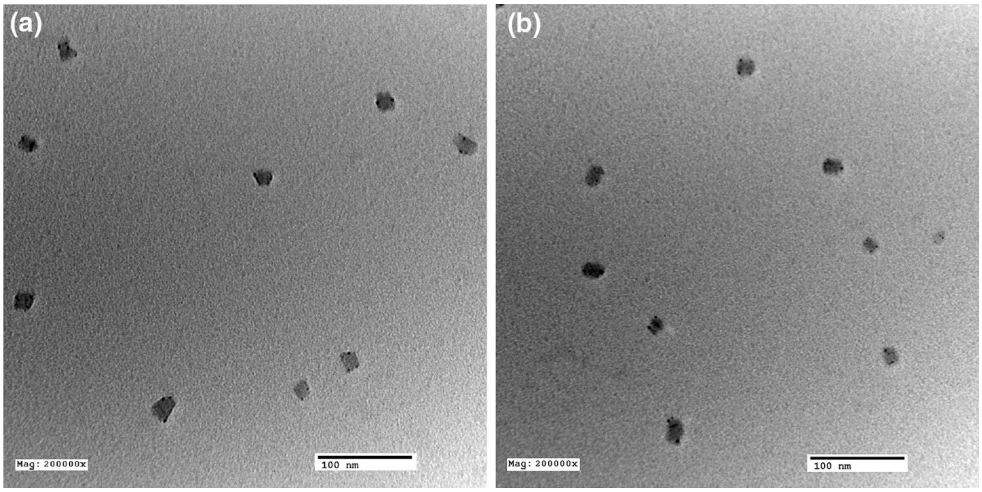


**Fig. 5** TEM images of **a** undoped and **b** 0.6 mol% Ni-doped $TiO_2$ nanoparticles

and doped sample is obtained as 20 nm and 15 nm, respectively. The TEM results are in correlation with the results obtained from XRD analysis, i.e., the particle size decreases with increase in dopant concentration, whereas negligible change in morphological structure is observed with increased doping. It is evident form Fig. 5 that the particles are nearly spherical in shape and uniformly distributed in both the cases. The estimated particle size obtained from XRD measurement is slightly higher as compared to the TEM measurement, which may be ascribed to the broadening of XRD peaks due to geometric reasons.

### Thermogravimetric analysis (TGA)

Thermogravimetric analysis is done in order to study the thermal stability of undoped $TiO_2$ as compared to nickel-doped $TiO_2$. Figure 6 shows the thermograms of undoped and Ni-doped $TiO_2$. The total weight loss in T0N, T2N, T4N and T6N samples is 1.21, 1.21, 3.01 and 1.45 %, respectively. T4N sample shows maximum weight loss among all the samples. The weight loss is attributed to the evaporation of water, volatility of organic compounds and loss of OH groups (Whang and Lim 2000). The samples show stable thermal behavior in terms of weight loss.

### Effect of doping on photocatalytic activity of $TiO_2$

To compare the photocatalytic activity of samples, a set of experiments was carried out for the degradation study of diethyl phthalate using T0N, T2N, T4N and T6N samples with irradiation time of 1 h and catalyst loading of 1 g/l for each experiment. The photocatalytic activity of the samples is determined by analyzing the extent of degradation of diethyl phthalate in each experiment for a fixed time and catalyst load. The initial concentration ($C_0$) of diethyl

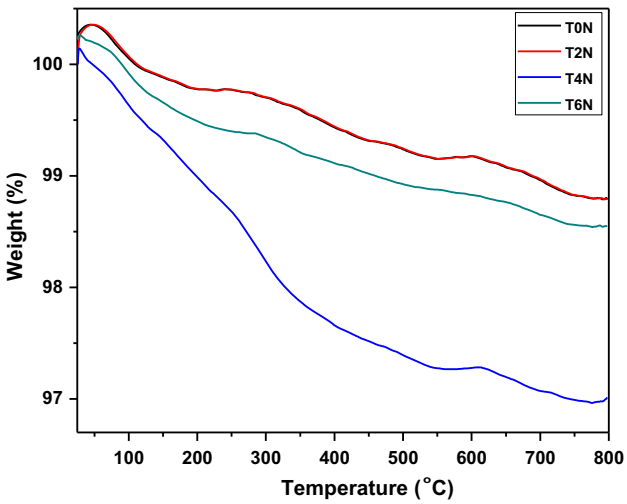


**Fig. 6** Thermograms of undoped and Ni-doped $TiO_2$ nanoparticles calcined at 450 °C

phthalate and dimethyl phthalate is taken to be 30 ppm, and the degradation percentage is calculated using the following equation (Aguilar et al. 2013):

$$\%D = \left(1 - \frac{A_t}{A_0}\right) \times 100 \quad (4)$$

where $A_0$ is the initial absorbance and $A_t$ is the absorbance after time t at $\lambda_{max}$. The degradation percentage of diethyl phthalate and dimethyl phthalate was maximum in case of T6N sample, which indicates that the photocatalytic activity of samples is increased with the increase in dopant concentration. Figure 7a, b shows a time-dependent UV–visible spectrum of diethyl phthalate and dimethyl phthalate solution using 0.6 mol% Ni-doped $TiO_2$ calcined at 450 °C during photoirradiation in the scanning range of 200–350 nm, respectively. In UV–Vis spectrum of diethyl

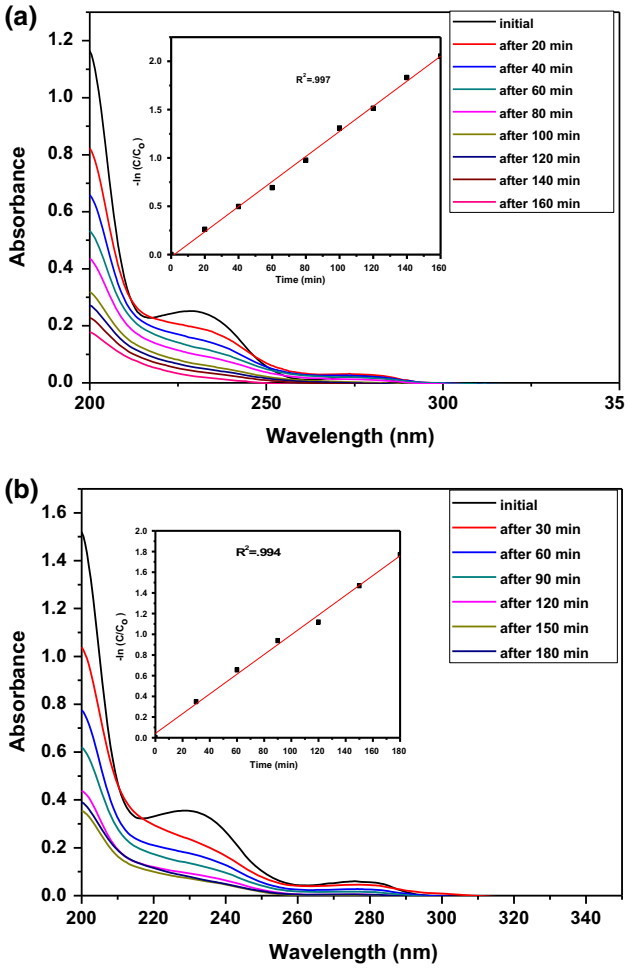


**Fig. 7** Degradation of **a** diethyl phthalate and **b** dimethyl phthalate during light irradiation in the presence of 0.6 mol% Ni–$TiO_2$ nanoparticles when $C_0 = 30$ ppm, catalyst load = 1 g/l

phthalate, two intense bands at wavelengths of 229 and 276 nm have been obtained. The decrease in absorption peak of diethyl phthalate at $\lambda_{max} = 229$ nm indicates complete degradation of diethyl phthalate during photodegradation. Almost similar results were obtained for dimethyl phthalate. In case of dimethyl phthalate, difference of one alkyl group as compared to diethyl phthalate does not give considerable change in UV–Vis spectrum of dimethyl phthalate. Degradation profile is also similar for dimethyl phthalate.

Inset of Fig. 7a, b shows kinetic study of degradation of diethyl phthalate and dimethyl phthalate, respectively. The dependency of rate of diethyl phthalate and dimethyl phthalate degradation on concentration of diethyl phthalate is described by Langmuir–Hinshelwood Kinetic model (Madhu et al. 2009), and the equation for pseudo-first order is:

$$-\ln\frac{C}{C_0} = k_{app}t \quad (5)$$

where $C_0$ is initial concentration of diethyl phthalate and dimethyl phthalate, $C$ is the concentration at irradiation time $t$ in ppm, respectively, and $k_{app}$ is the apparent rate constant. The linearity in graph in both the cases reveals that reaction is pseudo-first order.

## Conclusion

Doping of Ni in $TiO_2$ acts as crystallite size inhibitor and promotes the formation of anatase phase. The crystallite size of T0N, T2N, T4N and T6N samples is obtained to be approximately 28, 27, 25 and 22 nm, respectively. The value of Urbach energy increases with dopant concentration, indicating higher disorder in doped samples. However, band gap does not follow any trend with dopant concentration. The peak position shifts toward the lower wave number with the increase in Ni doping as has been observed in FTIR spectra. The TEM results are in correlation with the results obtained from XRD analysis, i.e., the particle size decreases with increase in dopant concentration, whereas negligible change in morphological structure is observed with increased doping. T6N sample shows the best photocatalytic activity due to the lowest crystallite size and higher disordering in this particular sample. Ni doping in $TiO_2$ has facilitated the degradation of phthalate esters.

**Acknowledgments** The authors are thankful to Dr. Gurbinder Kaur for her help in analyzing the results. Authors are also thankful to UGC for financial help under meritorious fellowships in reference to Letter No. F.4-1/2006/(BSR)/7-304/2010(BSR).

## References

Abbad MMB, Kadum AAH, Mohamad AB, Takriff MS, Sopian K (2012) Synthesis and catalytic activity of $TiO_2$ nanoparticles for photochemical oxidation of concentrated chlorophenols under direct solar radiation. Int J Electrochem Sci 7:4871–4888

Aguilar T, Navas J, Alcantara R, Lorenzo CF, Gallardo J, Blanco G, Calleja JM (2013) A route for the synthesis of Cu doped $TiO_2$ nanoparticles with very low band gap. Chem Phys Lett 571:49–53

Akpan UG, Hameed BH (2010) The advancements in sol–gel method of doped $TiO_2$ photocatalysts. Appl Catal A Gen 375:1–11

Ananpattarachai J, Kajitvichyanukul P (2015) Photocatalytic degradation of p,p′-DDT under UV and visible light using interstitial N-doped TiO2. J Environ Sci Health B 50:247–260. doi:10.1080/03601234.2015.999592

Chen C, Wang Z, Ruan S, Zhao M, Zou B, Wu F (2008) Photocatalytic degradation of C.I. Acid Orange 52 in the presence of Zn doped $TiO_2$ prepared by stearic acid gel method. Dyes Pigm 77:204–209

Cheng TS (2012) The toxic effects of diethyl phthalate on the activity of glutamine synthetase in greater duckweed (*Spirodelapolyrhiza* L.). Aquat Toxicol 2012(124–125):171–178

Chong MN, Jin B, Chow CW, Saint C (2010) Recent developments in photocatalytic water treatment technology: a review. Water Res 44:2997–3027

Devi LG, Murthy BN, Kumar SG (2010) Photocatalytic activity of $TiO_2$ doped with $Zn^{2+}$ and $V^{5+}$ transition metal ions: influence of crystallite size and dopant electronic configuration on photocatalytic activity. Mater Sci Eng B 166:1–6

Ding X, An T, Li G, Chen J, Sheng G, Fu J, Zhao J (2008) Photocatalytic degradation of dimethyl phthalate ester using novel hydrophobic $TiO_2$ pillared montmorillonite photocatalyst. Res Chem Intermed 34:63–83

Ebraheem S, Antar El-Saied (2013) Band gap determination from diffuse reflectance measurements of irradiated lead borate glass system doped with $TiO_2$ by using diffuse reflectance technique. Mater Sci Appl 4:324–329

Fairbairn EA, Bonthius J, Cherr GN (2012) Polycyclic aromatic hydrocarbons and dibutyl phthalate disrupt dorsal–ventral axis determination via the Wnt/β-catenin signaling pathway in zebrafish embryos. Aquat Toxicol 124–125:188–196

Ganesh I, Gupta AK, Kumar PP, Sekhar PSC, Radha K, Padmanabham G, Sundararajan G (2012) Preparation and characterization of Ni-doped $TiO_2$ materials for photocurrent and photocatalytic applications. Sci World J 2012:1–16

Ghasemi S, Rahimnejad S, Setayesh SR, Rohani S, Gholami MR (2009) Transition metal ions effect on the properties and photocatalytic activity of nanocrystalline $TiO_2$ prepared in an ionic liquid. J Hazard Mater 172:1573–1578

Hajjaji A, Atyaoui A, Trabelsi K, Amlouk M, Bousselmi L, Bessais B, Khakani MAE, Gaidi M (2014) Cr doped $TiO_2$ thin films prepared by means of a magnetron Co-sputtering process: photocatalytic application. Am J Anal Chem 5:473–482

Hanaor DAH, Sorrell CC (2011) Review of anatase to rutile transformation. J Mater Sci 46:855–874

He Z, Xiao H, Tang L, Min H, Lu Z (2013) Biodegradation of di-n-butyl phthalate by a stable bacterial consortium, HD-1, enriched from activated sludge. Bioresour Technol 128:526–532

Jamil TS, Gad Allah TA, Ali MEM, Momba MNB (2015) Utilization of nano size $TiO_2$ for degradation of phenol enrich water by solar photocatalytic oxidation. Desalin Water Treat 53:1101–1106

Jiana W, Joensa JA, Dionysioub DD, O'Sheaa KE (2013) Optimization of photocatalytic performance of $TiO_2$ coated glass microspheres using response surface methodology and the application for degradation of dimethyl phthalate. J Photochem Photobiol A Chem 262:7–13

Jing Y, Li L, Zhang Q, Lu P, Liu P, Lu X (2011) Photocatalytic ozonation of dimethyl phthalate with $TiO_2$ prepared by hydrothermal method. J Hazard Mater 189:40–47

Kaur G, Pandey OP, Singh K (2012) Effect of modifiers field strength on optical, structural and mechanical properties of lanthanum borosilicate glasses. J Non Cryst Solids 358:2589–2596

Kaur N, Kaur SS, Singh V (2015) Anomalous behavior of visible active $TiO_2$ for photocatalytic degradation of different reactive dyes. Photochem Photobiol Sci. doi:10.1039/C5PP00165J

Kumaresan L, Prabhu A, Palanichamy M, Arumugam E, Murugesan V (2011) Synthesis and characterization of $Zr^{4+}$, $La^{3+}$ and $Ce^{3+}$ doped mesoporous $TiO_2$: evaluation of their photocatalytic activity. J Hazard Mater 186:1183–1192

Liu W, Chen S, Zhao W, Zhang S (2009) Study on the photocatalytic degradation of trichlorfon in suspension of titanium dioxide. Desalination 249:1288–1293

Loan TT, Long NN (2014) Optical properties of anatase and rutile $TiO_2$:$Cr^{3+}$ powders. VNU J Sci Math Phys 30:59–67

Madhu GM, Antony Raj MAL, Pai KVK (2009) Titanium oxide ($TiO_2$) assisted photocatalytic degradation of methylene blue. J Environ Biol 30:259–264

Mansour E, El-Egili K, El-Damrawi G (2007) Ionic–polaronic behavior in $CeO_2$–$PbO$–$B_2O_3$ glasses. Phys B 39:221–228

Nahum AM, Raul OP, Roberto LR (2013) Removal of diethyl phthalate from water solution by adsorption, photo-oxidation, ozonation and advanced oxidation process ($UV/H_2O_2$, $O_3/H_2O_2$ and $O_3$/activated carbon). Sci Total Environ 442:26–35

Nakhate GG, Nikam VS, Kanade KG, Arbuj S, Kale B, Baeg JO (2010) Hydrothermally derived nanosized Ni doped $TiO_2$: a visible light driven photocatalyst for methylene degradation. Mater Chem Phys 124:976–981

Paul S, Choudhary A (2014) Investigation of the optical property and photocatalytic activity of mixed phase nanocrystalline titania. Appl Nanosci 4:839–847

Sarkar J, Chowdhury PP, Dutta TK (2013) Complete degradation of di-n-octyl phthalate by *Gordonia* sp. Strain Dop 5. Chemosphere 90:2571–2577

Singla P, Sharma M, Pandey OP, Singh K (2014) Photocatalytic degradation of azo dyes using Zn-doped and undoped $TiO_2$ nanoparticles. Appl Phys A 116:371–378

Staples CA (2003) Phthalate esters: the handbook of environmental chemistry. Springer, Berlin

Suwanchawalit C, Wongnawa S, Sriprang P, Meanha P (2012) Enhancement of the photocatalytic performance of Ag-modified $TiO_2$ photocatalyst under visible light. Ceram Int 38:5201–5207

Tain B, Li C, Zhang J (2012) One step reparation, characterization and visible light photocatalytic activity of Cr-doped $TiO_2$ with anatase and rutile bicrystalline phase. Chem Eng J 191:402–409

Tauc J, Menth A (1972) States in the gap. J Non Cryst Solids 8:569–585

Uddin MJ, Islam MA, Haque SA, Hasan S, Amin MSA, Rahman MM (2012) Preparation of nanostructured $TiO_2$ based photocatalysts by controlling the calcining temperature and pH. Int Nanolett 2:1–10

Umar K, Haque MM, Muneer M, Harada T, Matsumura M (2013) Mo, Mn, and La doped $TiO_2$: synthesis, characterization and photocatalytic activity for the decolourization of three different chromophoric dyes. J Alloys Compd 578:431–438

Venkatachalam N, Palanichamy M, Murugesan V (2007) Sol-gel preparation and characterization of alkaline earth metal doped nano $TiO_2$: efficient degradation of 4-chlorophenol. J Mol Catal A Chem 273:177–185

Vijayan P, Mahendiran C, Suresh C, Shanthi K (2009) Photocatalytic activity of iron doped nanocrystalline titania for the oxidative degradation of 2,4,6-trichlorophenol. Catal Today 141:220–224

Wang S, Lian JS, Zheng WT, Jiang Q (2012) Photocatalytic property of Fe doped anatase and rutile $TiO_2$ nanocrystal particles prepared by sol–gel technique. Appl Surf Sci 263:260–265

Wang CC, Li JR, Lv XL, Zhang YQ, Guo G (2014) Photocatalytic organic pollutants degradation in metal-organic frame works. Energy Environ Sci 7:2831–2867

Whang CM, Lim SS (2000) The effect of processing variables on structural changes and optical properties of $SiO_2$–$TiO_2$ sol-gel derived films. Bull Korean Chem Soc 21:1181–1186

Woo SH, Kim WW, Kim SJ, Rhee CK (2007) Photocatalytic behaviors of transition metal ions doped $TiO_2$ powder synthesized by mechanical alloying. Mater Sci Eng A 449–451:1151–1154

Wu Q, Liu H, Ye LS, Wang YH (2013) Biodegradation of Di-*n*-butyl phthalate esters by bacillus sp. SASHJ under simulated shallow aquifer condition. Int Biodeterior Biodegrad 76:102–107

Xu LJ, Chu W, Graham N (2013) A systematic study of the degradation of dimethyl phthalate using a high-frequency ultrasonic process. Ultrason Sonochem 20:892–899

Yang J, Bai H, Tan X, Lian J (2006) IR and XPS investigation of visible-light photocatalysis: nitrogen–carbon-doped $TiO_2$ film. Appl Surf Sci 253:1988–1994

Zaleska A (2008) Doped-$TiO_2$: a review. Recent Pat Eng 2:157–164